Journal of Materials Chemistry A

Accepted Manuscript

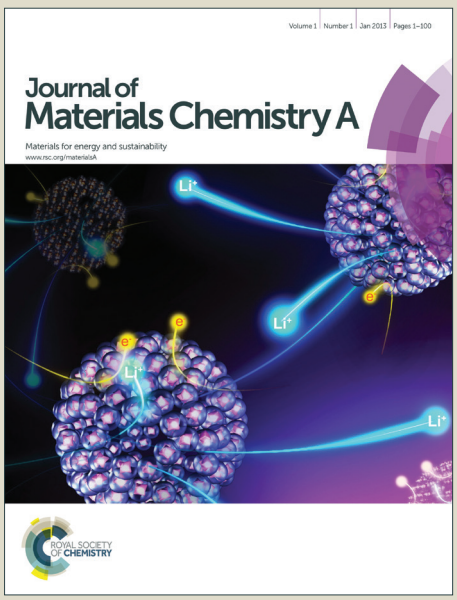

ROYAL SOCIETY OF CHEMISTRY

www.rsc.org/materialsA

Journal Name

RSCPublishing

PAPER

Gas Sensing Properties of Cu_2O and its Particle Size and Morphology-Dependent Gas-Detection Sensitivity

Xuejuan Wan,*[a, b, §] Jilei Wang,[a, b, §] Lianfeng Zhu[b] and Jiaoning Tang*[a]

Received (in XXX, XXX) Xth XXXXXXXXX 201X, AcceptedXth XXXXXXXXX 201X

DOI: 10.1039/b000000x

In order to investigate the effect of morphology and size on detection sensitivity towards ethanol vapor, nano-scale cubic or spherical Cu_2O with similar particle sizes were prepared through reductive solution chemistry routes. Experimental results indicated that both size and morphology of Cu_2O particles are playing important role in gas detection sensitivity, and the mutual competition and mutual dependence relations coexisted among the two factors. Particle morphology and morphology-dependent particle stacking mode may play a dominant role in relatively lower gas atmosphere (S_{50}, S_{260}> C_{50}, C_{340}). As the concentration of ethanol vapor exceeds 200 ppm, the size-dependent effect on gas-sensing gradually appears, that nanoparticles with relatively smaller particle size (C_{50}, S_{50} > C_{340}, S_{260}) possesses more advantageous in gas sensing process. At much higher ethanol partial pressure, Cu_2O nanoparticles with smaller size and cubic morphology exhibit strongest gas-sensing response. The mechanism of these gas-sensing divergences is suggested involving in the explanation of effective contact surface, width of charge accumulation layer (CAL) affected by gas concentration, energy bands bending changing and particle contact mode.

1. Introduction

Gas sensors play critical roles in monitoring environmental pollution, controlling industrial production, ensuring household and mining security. As a sort of important sensors, metal oxide semiconductor sensors have been considered promising ones due to their unique advantages, such as cost-efficiency, short response time, wide range of target gases and long lifetime, all of which are essential in our daily life. During the past decade, a great deal of attention has been focused on n-type semiconducting oxides, such as SnO_2,[1-8] In_2O_3,[9-12] Fe_2O_3,[13-16] ZnO[17-20] and WO_3,[21-29] while few studies focused on the factors that influence and control the behavior of p-type gas sensors although the architectures combined with n-type ones have been reported. Even at the present stage, researches on p-type gas sensors especially about Cu_2O is very scarce relative to Cr_2O_3,[30] Co_3O_4,[31, 32] V_2O_5 [33] and CuO.[34-36]

Copper (I) oxide (Cu_2O) (p-type) is an important metal oxide semiconductor showing remarkable catalytic properties and can be operated at relatively low temperatures comparing to n-type metal oxides. Moreover, it is possible to design and implement visible-light semiconductor photoelectric devices benefiting from their low bandgaps (~2.16 eV). While the large bandgap of n-type semiconducting metal oxides can only be tuned in the ultraviolet spectral range, which is not practical for the safe sensing applications.[37] In the field of gas-sensing, this type of semiconductor material has great potential in detecting pollutant gases due to its significant surface reactivity with both reducing and oxidizing gases, such as CO, SO_2, NO_2 and H_2S, which deserves deeper investigation. Further speaking, the sensor performance and fundamental understanding of Cu_2O nanoparticles are still in the elementary stage and further investigation is essential for improving the gas-sensing characteristics and elucidating the gas-sensing mechanism.

Due to the continuing enthusiasm for the synthesis of monodisperse nanoparticles with controlled morphologies, the exploration of the internal relationship between morphology and particle size and material performance has gained momentum. Up to now, numerous nanostructures of Cu_2O, including micro cubes,[38, 39] hollow-particles,[40, 41] nanoporous particles,[42] nanowires[43] and quasi-spherical[44] have been reported, together with pioneering research on their gas-sensing properties. All these works are extremely meaningful and very important for generating macro- or micro-novel structure so as to endow Cu_2O with more prominent and stable performance in the field of gas sensing. However, most researches mainly focused on optimizing the prescription and preparation of Cu_2O as well as other corresponding metal oxide particles. The cognizing and understanding for the gas-sensing mechanism is generally stayed on the basic working principle, which relied on the chemico-electrical transduction reactions that take place at the interface between molecular adsorbents and the metal oxide's surfaces.[45, 46] The effect of morphology and particles size on the gas-sensing performance of Cu_2O nanoparticles still remains an attractive challenge.

The gas-sensing performance is also closely related to the self-assembly and stacking mode of the sensor materials. For instance,

[a] Shenzhen Key Laboratory of Special Functional Materials, Engineering Laboratory for Advanced Technology of Ceramics, College of Materials Science and Engineering, Shenzhen University, Shenzhen 518060, PR China,

[b] Advanced Materials Institute, Graduate School at Shenzhen, Tsinghua University, Shenzhen 518055, PR China.

* Correspondence author. Tel: +86 0755 26534059; Fax: +86 0755 26534457; E-mail: wanxj@szu.edu.cn, tjn@szu.edu.cn

§ The two authors contributed equally to the work.

Zeng et al. prepared Cu_2O monolayer superlattices through a slow evaporation process, and this stacking mode is beneficial for elevating sensitivity and shortening response/recovery time.[47] Li et al. obtained three-dimensional self-assembly Cu_2O patterns by dip-coating method, leading to shortened response time (15s) to alcohol and lower detection limit.[48] The main explanation given in Li's report was that this stacking mode results in larger surface area and much more capacious inter-space, however Volanti et al. pointed out that the surface area is not the main source of the enhanced sensor response in their report.[49] These evidences indicate that the stacking mode may be a very important factor for improving gas-sensing response. Thus, the comparison of diverse Cu_2O samples for gas-sensing might be quite advantageous for the preliminary exploring of intrinsic sensing mechanism.

In this paper, four different Cu_2O nanoparticles with diverse morphology and particle size (Spherical, S_{260}, S_{50}, Cubic, C_{340}, C_{50}) were obtained through modified reductive solution chemistry routes at room temperature. The main discrepancies in gas-sensing performance of the obtained p-type Cu_2O sensor were compared and discussed in detail. Multiple factors containing effective contact surface, energy bands bending changing, the width of charge accumulation layer affected by gas concentration and contact mode were considered which may be helpful for understanding the impacts on gas-sensing performance caused by material's stacking or self-assembling.

2. Experimental

2.1 Chemicals

Cupric (II) acetate monohydrate ($(CH_3COO)_2Cu{\cdot}H_2O$) and hydrazine hydrate ($N_2H_4{\cdot}H_2O$, 50%) were purchased from Sinopharm Chemical Reagent Company. Poly(N-vinylpyrrolidone) (PVP, Wt = 40000) and poly(ethylene glycol) (PEG, Wt = 400) were provided by Sigma-Aldrch. L-Ascorbicacid (AA, AR, 98%), sodium tetrahydridoborate ($NaBH_4$, AR, 98%) and sodium hydroxide (NaOH, AR, 96%) were obtained from Alfa Aesar, Cantotech, Aladdin Industrial Corporation, respectively. All the reagents were used as received without any further purification.

2.2 Synthesis of Cu_2O Nanocubes

Cu_2O nanocubes were prepared through a modified reductive solution chemistry route. Typical procedure can be described as follows: solution A was prepared by mixing 20 mL PEG_{400} (0.05 mol/L) and 40 mL $(CH_3COO)_2Cu{\cdot}H_2O$ (0.01 mol/L) aqueous solution. Solution B was prepared by mixing 20 mL AA (0.1 mol/L), 60 mL NaOH (0.5 mol/L) aqueous solution and 380 mL deionized water. Under N_2 atmosphere, solution B was added quickly into solution A with vigorous stirring at room temperature. Upon addition, the mixture immediately changed to orange colour. After the reaction was terminated 40 min later, C_{50} was recovered by repeated centrifuging-washing cycles with distilled water and ethanol, drying in a vacuum at 60 °C for 12 h. When NaOH was added dropwise into solution A (about 10 min) first and AA was added 1 minute later with the same injection rate, C_{340} was obtained, with all other conditions remaining the same as the procedure for C_{50}.

2.3 Synthesis of Cu_2O Nanospheres

A typical procedure for synthesizing Cu_2O nanospheres was carried out as follows: 20.0 mg $(CH_3COO)_2Cu{\cdot}H_2O$ was dissolved in 60.0 mL isopropanol. The capping agent，200 mg PVP was then added into the above solution mixture. Afterward, 5.0 mL NaOH solution (0.2 M, in isopropanol) was added under vigorous magnetic stirring in 10 min, followed by dropping 0.3 mL $N_2H_4{\cdot}H_2O$ and stirred for another 10 min. Upon addition, the emerald green solution turned deep orange-red, indicating the formation of Cu_2O colloid in oxygen atmosphere. Finally, S_{50} was recovered by centrifuging-washing cycles with distilled water and ethanol, drying in a vacuum at 60 °C for 12 h. S_{260} was prepared by adjusting the solution pH up to 10 with dropwise addition of 1 M NaOH solution. The solvent and reducing agent was replaced by deionized water and $NaBH_4$ (3.0 mL, 0.5 M) respectively.

2.4 Gas Sensor Application for Ethanol Detection

2.0 mg Cu_2O sample was mixed with ethanol (30 μL) in order to form a slurry. Afterward the slurry was pasted uniformly on the external surface of the ceramic platform of the sensors. The sample was suspended with Pt wires to form heat insulation structure. Desired constant operating temperatures could be obtained by applying certain voltages to the heater. The substrate temperature was measured with a thermocouple. The electrical currents of the particles were monitored using a Digital Multimeter (Victor 86B), with a constant dc voltage of 5.0 V. The responses of gas sensors in dry air were tested by gas distribution method. Customized gastight chamber with fixed volume of 10 L was used. Tested sensor was mounted in the chamber with conducting wire leading out of the gastight chamber. The accurate current was recorded after putting the sensors at a working temperature of 200°C into the gas chamber, which was charged with ethanol vapor at different concentrations.

2.5 Characterization

Transmission electron microscopic (TEM) images of the Cu_2O nanocrystals were taken on a JEOL-3000F electron microscope. TEM samples were prepared by dropping the nanocrystal solution onto a carbon coated copper grid. Scanning electron microscopic (SEM) images were taken on a Hitachi-S4800FESEM attached with energy dispersive X-ray spectroscopy (EDX). X-Ray powder diffraction (XRD) was carried out using an XRD-6000 (Japan) X-ray diffractometer with Cu–Karadiation (λ=1.54060Å) at a scanning rate of 5.0°/min.

3. Results and discussion

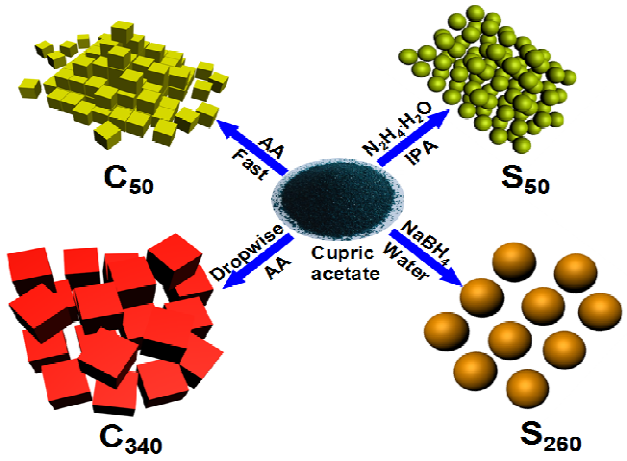

Scheme 1 Schematic illustration for the formation process of Cu_2O nanoparticles with different morphology and size.

A convenient modified solution-phase method has been selected for the controlled syntheses of Cu_2O cubic and spherical crystals with various sizes in this paper. The formation pathway of these four sized nanoparticles via different reaction systems were illustrated in Scheme 1. The morphology and size of the as-prepared Cu_2O are greatly influenced by their reacting conditions, such as solvent, the rate of oxidation-reduction process, and especially the choosing of reducing agent. Generally, Cu_2O particles are prepared by reducing

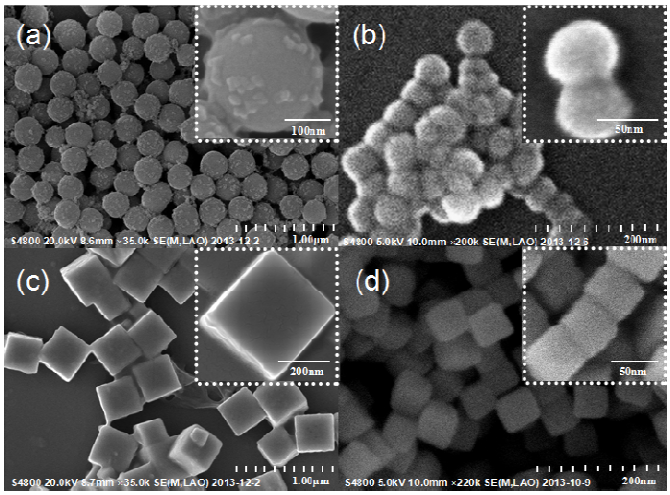

Fig. 1 SEM images of Cu_2O nanoparticles with different morphology and size, (a) S_{260}, (b) S_{50}, (c) C_{340}, (d) C_{50} and insets are the corresponding magnified images.

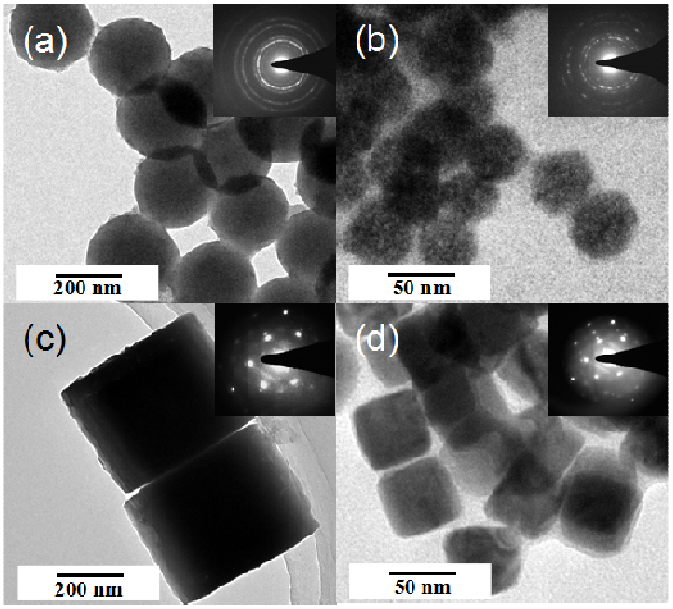

Fig. 2 TEM images and SAED patterns of different Cu_2O nanoparticles. (a) S_{260}, (b) S_{50}, (c) C_{340}, (d) C_{50}

$Cu(OH)_2$ precipitates with AA or $NaBH_4$ in water, or $N_2H_4{\cdot}H_2O$ in isopropanol. Once the reducing agent was added into the reaction mixture, seed particles were formed immediately and then aggregated. Simultaneously, the aggregations would undergo a surface reconstruction to evolve into a cubic morphology under weak redox condition (C_{50} or C_{340}) and this postulation has been confirmed in previous reports.[50] But there's not enough time to re-adjust the structure of Cu_2O crystals in a strong redox system and the surface reconstruction is also difficult to happen. Therefore, spherical Cu_2O is most likely to be obtained in the presence of strong reducing agent $NaBH_4$ or hydrazine hydrate (S_{50} or S_{260}).

The representative morphology and size of the obtained Cu_2O samples were revealed by SEM and TEM measurements. Fig. 1a, Fig. 2a show the SEM and TEM image of the sample obtained using $NaBH_4$, which indicates that this sample is composed of many spherical crystals with average grain size about 260 nm. As the reducing agent was replaced by $N_2H_4{\cdot}H_2O$, S_{50} maintaining high monodispersivity were obtained in isopropanol (Fig 1b and Fig 2b). Additionally, Cu_2O nanocubes with different sizes (C_{340}, Fig. 1c, Fig. 2c, C_{50}, Fig. 1d, Fig. 2d) have been generated through adjusting the adding modes of reducer ascorbic acid (AA) and sodium hydroxide (NaOH). When AA and NaOH were added dropwise into solution A sequentially, larger Cu_2O nanocubes with an edge length of about 340nm were obtained. As AA and NaOH were quickly added into solution A simultaneously, C_{50} could be generated.

SAED patterns indicate that the S_{260} and S_{50} particles are polycrystalline and C_{50} and C_{340} are single-crystalline with highly oriented in the scale of selected area. (Fig. 2) EDX shows the elemental mapping of Cu, and the more centralized distribution of Cu may indicate the more tightly packing between particles. (Fig. 3) The X-ray diffraction (XRD) patterns (in Fig. 4) show that all the diffraction peaks of the as-obtained Cu_2O nanoparticles agree perfectly with those of cubic Cu_2O standard card (JCPDS card no. 05-0667). Specially, the strong and sharp peaks observed in cubic nanoparticles indicate that the obtained Cu_2O crystals are highly crystalline.

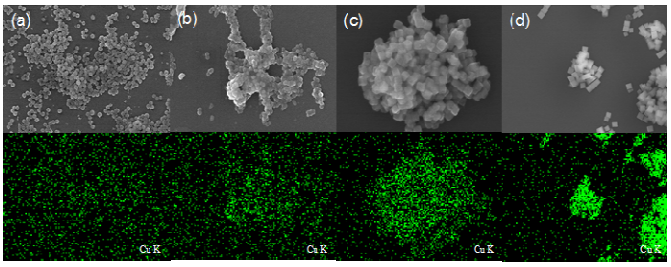

Fig. 3 SEM images and corresponding EDX elemental mapping of Cu, (a) S_{260}, (b) S_{50}, (c) C_{340}, (d) C_{50}

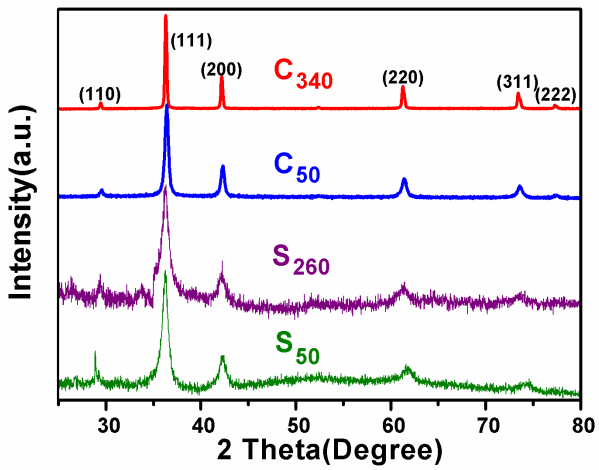

Fig. 4 X-ray diffraction (XRD) patterns of Cu_2O nanoparticles with different morphology and size.

Fig. 5 (a), (b) shows the photograph of the gas sensor and four different Cu_2O nanoparticles dispersed in ethanol. The colour of

Cu_2O dispersion was changed from brick-red to yellow-green accompanied with the alteration of particle size due to size-dependent scattering. Gas sensor devices mainly consists of four major components as shown in Fig. 5(c): resistance heater, ceramic platform, Pt wire, and Au electrode. Four Cu_2O nanoparticles were assembled on the ceramic platform by dip-coating respectively, and the responses of gas sensors were tested by a stationary state gas distribution method.Typical SEM image of the surface structure after

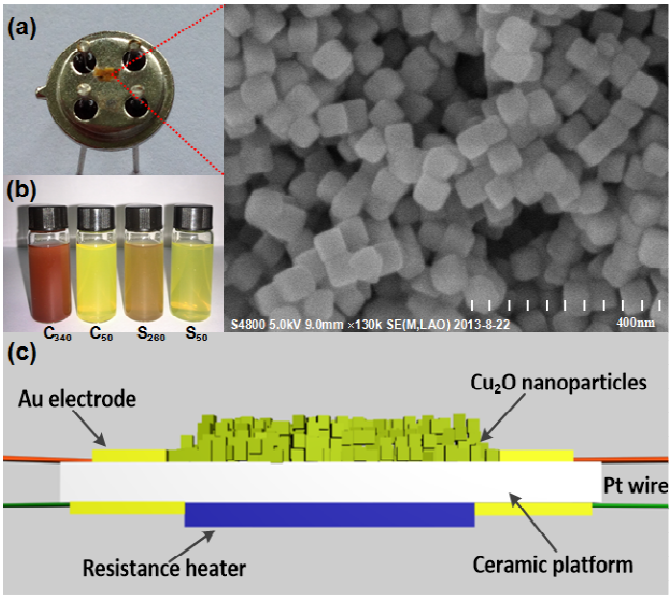

Fig. 5 Photograph of the gas sensor and four different Cu_2O nanoparticles dispersed in ethanol and the corresponding SEM image of thin films coated on it (a) (b), and schematic diagram showing the structure of a typical Cu_2O nanoparticles gas sensor by sectional view (c).

Cu_2O coating (C_{50}) was shown in Fig. 5(a right), suggesting that the morphology of the samples was well-maintained during the dip-coating process. The resistance variations of the obtained sensors in air or ethanol vapor were measured by monitoring output current. Semiconductor metal oxide gas sensors are generally operated at elevated temperatures (100–400°C) in order to accelerate chemical reactions between metal oxide surface and target gas molecules. Considering the balance between relative lower energy consumption and appropriate detection sensitivity,[39,48] 200°C is selected as the working temperature to test the gas-sensing performance.

Fig. 6 shows the typical isothermal response curves of Cu_2O when cycled by increasing alcohol vapor in ambient air with the range of 50-800 ppm, at a working temperature of 200°C. Their sensitivities to alcohol have been demonstrated in Fig. 7. The gas sensitivity is defined as R_g/R_a, where R_g and R_a are the resistances of the sensor respectively in ethanol vapor and air atmosphere at 200 °C. From these results, it is evident that the sensitivity of C_{50} increases from 2.64 to 3.91 with the concentration of ethanol vapor increasing from 350 to 800 ppm, higher than that (from 2.64 to 3.39) of S_{50}. While, the sensitivity values of S_{50} increase from 1.74 to 2.64, as ethanol vapor increased from 50 to 350 ppm, which was higher than that (from 1.38 to 2.64) of C_{50}. Both S_{260} and C_{340} displayed relatively lower sensitivity (from 1.77 to 2.51 and from 1.52 to 2.47), and C_{340} displayed higher sensitivity than S_{260} when the gas concentration exceeds 200 ppm. This phenomenon was reasonable based on a conduction model which mainly focuses on the active sensing layer (Debye-layer) resistance and the grain-to-grain contact resistance, both of which are gas sensitive.[51] Gas response increases with increasing neck diameter (D_N, Fig. 8), when the grain size (D_G) was constant, suggesting that the effective contact area between the adjacent Cu_2O particles is an important parameter to determine the gas response in p-type gas sensors and the similar postulation were confirmed by Lee et al.[52] Generally, particles possessing comparable size but diverse morphology will display striking different effective contact surface. Obviously, cubic Cu_2O nanoparticles have a larger D_N and contact area than spherical Cu_2O nanoparticles when they have similar particle size, thus better gas-sensing sensitivity was obtained. As for the size factor, the bigger the particle sizes are, the smaller the effective contact surface will become per unit volume, which was both true for cubic particles and spherical particles. This also means particles with relatively smaller size may have more advantageous in ethanol vapour sensing.

Based on the model mentioned above, the surface reactivity is essential deserving to a simple elaboration. It is generally considered that the surface ionosorbed oxygen species act as gas acceptor, and the reduction reaction between the ethanol vapor and acceptor will occurred in the sensing process. Thus, the variation of acceptor density is responsible for gas detection sensitivity. The oxygen acceptors bind electron, resulting in the appearance of a charge accumulation layer (CAL) for holes. The width of CAL (L_D) is modulated by the capture and release of electrical charges, and this will further modify the height of energy barrier between the adjacent two particles.

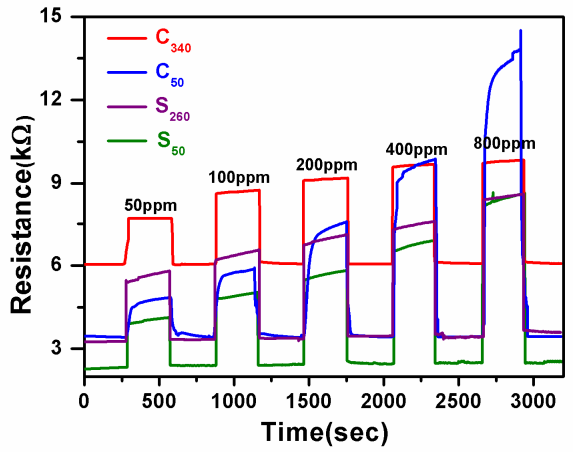

Fig. 6 Dynamic response-recovery curves of the gas sensor based on different Cu_2O nanoparticles toward absolute alcohol vapor with increasing concentrations at 200 °C.

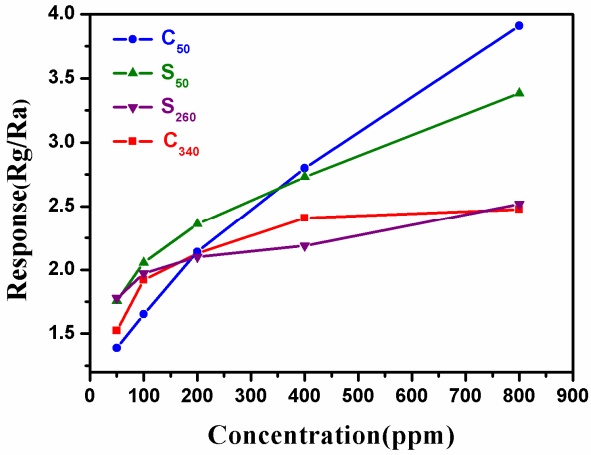

Fig. 7 The relationship between response (Rg/Ra) of various Cu_2O samples and different gas concentrations.

Fig. 8 left, depicts that the variation of the L_D was considered to be associated to the adsorption of ambient oxygen with negative charge. The CAL was built up resulting from the increase of holes concentration in the vicinity of the surface, which can be illustrated in an upward bending of the energy band. When exposed in ethanol (Fig. 8 right), the ethanol molecules reduce the oxygen acceptor and injected electrons into the CAL. Consequently, holes are partially neutralized and L_D decreased, which further leads to a lower energy barrier between two particles. These significant discrepancies of response shown in Fig. 7 could be explained with the different D_N (neck diameter) existing in contact zone which may has a close relationship with the particle stacking mode and L_D depicted in Fig. 8. Compared to the case for spherical particles with point-to-point contacting, higher ethanol partial pressure is necessary for ethanol molecules overcoming the higher permeating barriers of cubic particles with face-to-face contacting. Once the ethanol molecules arrive at the contact zone of cubic particles of face-to-face contacting and reduce the density of oxygen accepter, a larger D_N is obtained. Thus a stronger gas-sensing response is observed. And this was also in accordance with the detection results displaced in Fig.7, that spherical Cu_2O exhibit larger detection sensitivity than cubic Cu_2O at lower gas concentration, while the situation was opposite as the concentration of ethanol vapor increased. Overall, the ethanol detection sensitivity was determined by the L_D and D_N. The latter was much influenced by particle stacking mode which was finally decided by the particle morphology and size.

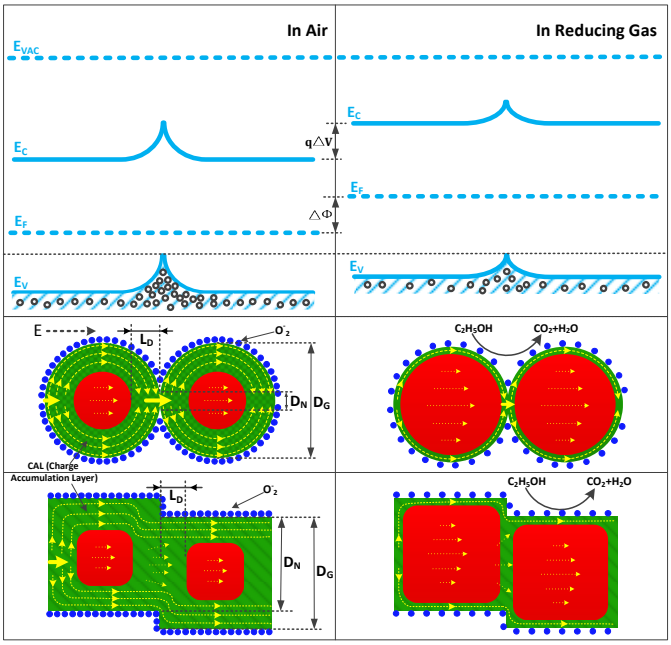

Fig. 8 Energy bands representation of the surface processes associated to the reaction with ambient oxygen (left) and reducing gases (right). E_{VAC} is the energy level of the electrons far away from the semiconductor; E_C is the minimum of the conduction band; E_V is the maximum of the valence band; Φ is the work function and $q\Delta V = \Delta\Phi$ (L_D, Debye length, D_N, size of neck, D_G, size of particle).

4. Conclusions

Cu_2O nanocubes and nanospheres were prepared through modified reductive solution chemistry routes at room temperature. These four different particles were used to assemble chemical gas sensor, which shows striking discrepancies of gas sensitivity. Experimental results indicated that the sensitivity trend is: cubic Cu_2O of *ca.* 50 nm (C_{50}) > spherical Cu_2O of *ca.* 50 nm (S_{50}) > cubic Cu_2O of *ca.* 340 nm (C_{340}) > spherical Cu_2O of *ca.* 260 nm (S_{260}) at relatively higher ethanol partial pressure; $S_{50} > S_{260} > C_{340} > C_{50}$ at lower ethanol vapor concentration (< 200 ppm). Since the gas detection sensitivity was determined by the charge accumulation layer and neck diameter between two particles, particle morphology and size and the corresponding particle stacking mode of Cu_2O played an essential role in the gas-sensing capacity. These results may contribute to modulate relevant experimental parameters for preparing p-type semiconductors gas sensing with exceptional performance.

Acknowledgements

The financial support from National Natural Scientific Foundation of China (NNSFC) Project (21204042), Fundamental Research Project of Shenzhen (JCYJ20120830152316443), Technology Innovation Program of Shenzhen (CXZZ20130322101824104), National High Technology Research and Development Program of China (863 Program, 2012AA030312), and China Postdoctoral Science Foundation (2013M530614) are gratefully acknowledged. Prof. Yao Youwei of Tsinghua University is greatly appreciated for his valuable suggestions.

Notes and references

1. Z. Li, Q. Zhao, W. Fan and J. Zhan, *Nanoscale*, 2011, **3**, 1646.
2. A. Kolmakov, D. Klenov, Y. Lilach, S. Stemmer and M. Moskovits, *Nano Letters*, 2005, **5**, 667.
3. J. Cao, T. Zhang, F. Li, H. Yang and S. Liu, *New J. Chem.*, 2013, **37**, 2031.
4. S. Tian, X. Ding, D. Zeng, J. Wu, S. Zhang and C. Xie, *RSC Adv.*, 2013, **3**, 11823.
5. X. Wang, S. Qiu, C. He, G. Lu, W. Liu and J. Liu, *RSC Adv.*, 2013, **3**, 19002.
6. W. Göpel and K. D. Schierbaum, *Sens. Actuators B: Chem.,* 1995, **26**, 1.
7. T. Jinkawa, G. Sakai, J. Tamaki, N. Miura and N. Yamazoe, *J. Mol. Catal. A: Chem.*, 2000, **155**, 193.
8. N. Barsan, M. Schweizer-Berberich and W. Göpel, *Fresenius' J. Anal. Chem.*, 1999, **365**, 287.
9. Z. Zhuang, Q. Peng, J. Liu, X. Wang and Y. Li, *Inorg. Chem.*, 2007, **46**, 5179.
10. G. Han, Q. Lu, G. Liu, X. Ye, S. Lin, Y. Song, B. Liu, X. Yang and G. Li, *J. Mater. Sci. - Mater. Electron.*, 2012, **23**, 1616.
11. C. Zhao, G. Zhang, W. Han, J. Fu, Y. He, Z. Zhang and E. Xie, *CrystEngComm*, 2013, **15**, 6491.
12. B. Li, Y. Xie, M. Jing, G. Rong, Y. Tang and G. Zhang, *Langmuir*, 2006, **22**, 9380.
13. P. Sun, X. He, W. Wang, J. Ma, Y. Sun and G. Lu, *CrystEngComm*, 2012, **14**, 2229.
14. S. Zhang, F. Ren, W. Wu, J. Zhou, X. Xiao, S. Lingling, Y. Liu and C. Jiang, *Phys. Chem. Chem. Phys.*, 2013, **15**, 8228.
15. J. Ma, L. Mei, Y. Chen, Q. Li, T. Wang, Z. Xu, X. Duan and W. Zheng, *Nanoscale*, 2013, **5**, 895.
16. P. Sun, Z. Zhu, P. Zhao, X. Liang, Y. Sun, F. Liu and G. Lu, *CrystEngComm*, 2012, **14**, 8335.
17. G. C. Qi, L. Zhang and Z. H. Yuan, *Phys. Chem. Chem. Phys.*, 2014, DOI: 10.1039/C4CP00906A.
18. J. Xu, Q. Pan, Y. a. Shun and Z. Tian, *Sens. Actuators B: Chem.*, 2000, **66**, 277.
19. N. Hongsith, E. Wongrat, T. Kerdcharoen and S. Choopun, *Sens. Actuators B: Chem.*, 2010, **144**, 67.
20. D. Barreca, E. Comini, A. P. Ferrucci, A. Gasparotto, C. Maccato, C. Maragno, G. Sberveglieri and E. Tondello, *Chem. Mater.*, 2007, **19**, 5642.
21. T. Inoue, K. Ohtsuka, Y. Yoshida, Y. Matsuura and Y. Kajiyama, *Sens. Actuators B: Chem.*, 1995, **25**, 388.
22. C. Zhang, A. Boudiba, P. De Marco, R. Snyders, M. G. Olivier and M. Debliquy, *S Sens. Actuators B: Chem.*, 2013, **181**, 395.

23. D. Chen, L. Yin, L. Ge, B. Fan, R. Zhang, J. Sun and G. Shao, *Sens. Actuators B: Chem.*., 2013, **185**, 445.
24. Y. K. Chung, M. H. Kim, W. S. Um, H. S. Lee, J. K. Song, S. C. Choi, K. M. Yi, M. J. Lee and K. W. Chung, *Sens. Actuators B: Chem.*, 1999, **60**, 49.
25. M. Tong, G. Dai, Y. Wu, X. He and D. Gao, *J. Mater. Sci.*, 2001, **36**, 2535.
26. X. L. Li, T. J. Lou, X. M. Sun and Y.-D. Li, *Inorg. Chem.*, 2004, **43**, 5442.
27. J. Lee, O. S. Kwon, D. H. Shin and J. Jang, *J. Mater. Chem. A*, 2013, **1** , 9099.
28. X. Li, G. Zhang, F. Cheng, B. Guo and J. Chen, *J. Electrochem.. Soc.*, 2006, **153**, 133.
29. D. Chen, X. Hou, H. Wen, Y. Wang, H. Wang, X. Li, R. Zhang, H. Lu, H. Xu and S. Guan, *Nanotechnology*, 2010, **21**, 1.
30. S. Pokhrel, C. Simion, V. Quemener, N. Barsan and U. Weimar, *Sens. Actuators B: Chem.*, 2008, **133**, 78.
31. K. I. Choi, H. R. Kim, K. M. Kim, D. Liu, G. Cao and J. H. Lee, *Sens. Actuators B: Chem.*, 2010, **146**, 183.
32. D. Patil, P. Patil, V. Subramanian, P. A. Joy and H. S. Potdar, *Talanta*, 2010, **81**, 37.
33. M. Yu, X. Liu, Y. Wang, Y. Zheng, J. Zhang, M. Li, W. Lan and Q. Su, *Appl. Surf. Sci.*, 2012, **258**, 9554.
34. Y. J. Chen, F. N. Meng, H. L. Yu, C. L. Zhu, T. S. Wang, P. Gao and Q. Y. Ouyang, *Sens. Actuators B: Chem.*, 2012, **176**, 15.
35. Y. H. Choi, D. H. Kim, S. H. Hong and K. S. H, *Sens. Actuators B: Chem.*, 2013, **178**, 395.
36. L. Liao, Z. Zhang, B. Yan, Z. Zheng, Q. Bao, T. Wu, C. Li, Z. Shen, J. Zhang and H. Gong, *Nanotechnology*, 2009, **20**, 1.
37. A. S. Zoolfakar, M. Z. Ahmad, R. A. Rani, J. Z. Ou, S. Balendhran, S. Zhuiykov, K. Latham, W. Wlodarski, K. Kalantar-zadeh, *Sens. Actuators B: Chem.*, 2013, **185**, 620.
38. L. Zhang, H. Li, Y. Ni, J. Li, K. Liao and G. Zhao, *Electrochem. Commun.,* 2009, **11**, 812.
39. X. W. Liu, F. Y. Wang, F. Zhen and J.-R. Huang, *RSC Advances*, 2012, **2**, 7647.
40. Z. Gao, J. Liu, J. Chang, D. Wu, J. He, K. Wang, F. Xu and K. Jiang, *CrystEngComm*, 2012, **14**, 6639.
41. H. Zhang, Q. Zhu, Y. Zhang, Y. Wang, L. Zhao and B. Yu, *Adv. Funct. Mater.*, 2007, **17**, 2766.
42. Y. Zhao, Y. Li, Z. He and Z. Yan, *RSC Advances*, 2013, **3**, 2178.
43. S. Deng, V. Tjoa, H. M. Fan, H. R. Tan, D. C. Sayle, M. Olivo, S. Mhaisalkar, J. Wei and C. H. Sow, *J. Am. Chem. Soc.*, 2012, **134**, 4905.
44. J. Liu, S. Wang, Q. Wang and B. Geng, *Sens. Actuators B: Chem.*, 2009, **143**, 253.
45. G. Korotcenkov, *Sens. Actuators B: Chem.*, 2005, **107**, 209.
46. E. Comini, C. Baratto, G. Faglia, M. Ferroni, A. Vomiero and G. Sberveglieri, *Prog. Mater Sci.,* 2009, **54**, 1.
47. K. X. Yao, X. M. Yin, T. H. Wang and H. C. Zeng, *J. Am. Chem. Soc.*, 2010, **132**, 6131.
48. J. Zhang, J. Liu, Q. Peng, X. Wang and Y. Li, *Chem. Mater.*, 2006, **18**, 867.
49. D. P. Volanti, A. A. Felix, M. O. Orlandi, G. Whitfield, D. J. Yang, E. Longo, H. L. Tuller and J. A. Varela, *Adv. Funct. Mater.*, 2012, **23**, 1759.
50. C. H. Kuo, C. H. Chen and M. H. Huang, *Adv. Funct. Mater.*, 2007, **17**, 3773.
51. N. Barsan, C. Simion, T. Heine, S. Pokhrel and U. Weimar, *J Electroceram*, 2010, **25**, 11.
52. J. W. Yoon, J. K. Choi and J. H. Lee, *Sens. Actuators B: Chem.*, 2012, **161**, 570.